Claremont Colleges
Scholarship @ Claremont

Scripps Senior Theses

Scripps Student Scholarship

2015

Comparing Bulk Aerosol Profiles in the Mixed Layer in Coastal Los Angeles and the Inland Empire

Taia Sean Wu
Scripps College

Recommended Citation

Comparing bulk aerosol profiles in the mixed layer in coastal Los
Angeles and the Inland Empire

A senior thesis in Chemistry

by

Taia Sean Wu

Table of contents

Figures and tables

Equations

Abstract

Characteristic westerly sea breeze carries air over the Los Angeles Basin in Southern California to the Inland Empire approximately 50 miles inland, directly impacting air quality in both of these two highly polluted regions. As particles play a critical role in air quality and human health, this study compares the bulk aerosol profiles of the Los Angeles pollution "source" and Inland Empire "receptor" regions during the 2013 and 2014 NASA Student Airborne Research Program (SARP) campaigns onboard the NASA DC-8 airborne laboratory. The source and receptor regions were characterized by a series of missed approaches at the Los Angeles International Airport, Long Beach Airport, and Los Alamitos Army Airfield (coastal sources) as well as the Ontario International Airport, San Bernardino International Airport, and March Air Reserve Base (inland receptors). The aerosol populations in each region were compared, and the changes evolved were analyzed alongside volatile organic compound (VOC) concentrations from Whole Air Samples. Particle size distributions were collected using a Droplet Measurement Technologies Ultra High Sensitivity Aerosol Spectrometer (DMT-UHSAS). Aerosol concentration, mass, and mode diameter increased significantly between coastal pollution source and inland pollution receptor regions in all cases, along with an increase in mode diameter. The observed changes cannot be accounted for by aerosol aging over the Los Angeles basin alone, suggesting new particle emission/formation over this region could be a dominating factor in the changes. Positive correlations between particle increases at receptor sites and anthropogenic VOC tracers will be discussed.

Introduction

Atmospheric aerosols: an introduction

An aerosol is a small solid or liquid particle suspended in a gas, ranging in diameter from 2nm-100μm. Atmospheric aerosol is generally classified into two source-distinct categories[1]: primarily organic aerosol (POA) and secondary organic aerosol (SOA), though many sub-classifications exist as well. POA is introduced into the atmosphere via direct emission from sources such as waves crashing onto the shore[2], motor traffic[3], cooking, and biomass burning.[4] POA generally contributes to the larger (>800nm diameter) end of the aerosol spectrum[5]. SOA is formed from the nucleation of low-volatility gases in the atmosphere[6]. These condensable gases are produced upon photo-oxidation of gaseous volatile organic compounds (VOCs). Aerosol is a key component of urban air pollution and significantly impact both climate and human health, with specific effects depending on particle composition and diameter.

Tropospheric aerosols scatter light, cooling the planet in an effect known as "radiative forcing."[7] Aerosols also serve as cloud condensation nuclei[5]. In doing so, they alter cloud cover[8] and reflective properties[9] as well as perturb the natural hydrological cycle, including the suppression of rainfall[10]. A main component of urban smog, aerosols are responsible for reduced visibility in many heavily-populated cities[11–13]. In Los Angeles, this effect regularly shortens the visible distance to less than 10km[11,14,15]—a more than ten-fold decrease from that of clean air, and a five-fold reduction from a typical European city[16].

Epidemiological studies have connected aerosols to a variety of severe health issues[17–20]. Multiple studies nation-wide directly link temporal peaks in urban aerosol to increased mortality from cardiovascular and respiratory illnesses[21–23]. In 1999, Etzel et al. correlated days with heightened aerosol density to increases in cardio-pulmonary related high school absences[24]. Heightened aerosol concentrations in diminish lung health and stunt lung development in children[25,26] as well as induce new cases of asthma and aggravate pre-existing bronchial conditions[18]. Recent studies have found that aerosols containing ferrous and quinone species cause mitochondrial dysfunction[27,28].

Biological responses to aerosols vary with particle size[12,18]. Toxicity generally increases with decreasing diameter[17,23,29,30]. 90-99 percent of urban aerosol concentration resides in the 0-100nm "ultrafine" range[31–34]; recent studies suggest this range may be especially harmful[27,28]. However, ultrafine aerosol remains largely unregulated, in part due to the technical difficulty of measuring at these diameters.

Southern California has some of the highest concentrations of ultra-fine aerosol in the country[18] and

regularly exceeds EPA standards[21,35,36], with the 98th percentile of $PM_{2.5}$ daily maxima in Los Angeles exceeding the EPA standard of 35µg m^{-3} every year from 1999-2007[3.7] The US Environmental Protection Agency (US EPA) estimates that 400,000 cases of respiratory illness in children could be prevented annually in California if the new annual ultra-fine ambient aerosol average of <12µg m^{-3} were met[38] and results from the California Children's Health Aerosol Studies[18] suggest that the long-term benefits of complying with such regulations may be even greater than the current state estimates[38–40].

Given the pertinence of aerosol to climate, health, and corresponding regulations, monitoring urban aerosol size distributions and concentrations is crucial. However, the complexity of atmospheric interactions[41,4243–50] and aerosol sources[51] render models highly speculative[52–54], and recent studies have found that aerosol concentrations are often dramatically under-predicted[37,55], Topographic variability and complex human activity make Southern California aerosol particularly difficult to predict. Few models can resolve different locations in the Los Angeles Basin[1], though aerosol over heavily traffic-influenced cities can be highly varied[56–58]. Thus, in-situ measurements of this area remain critical for both health and climate safety.

Aerosol in Los Angeles and the Inland Empire
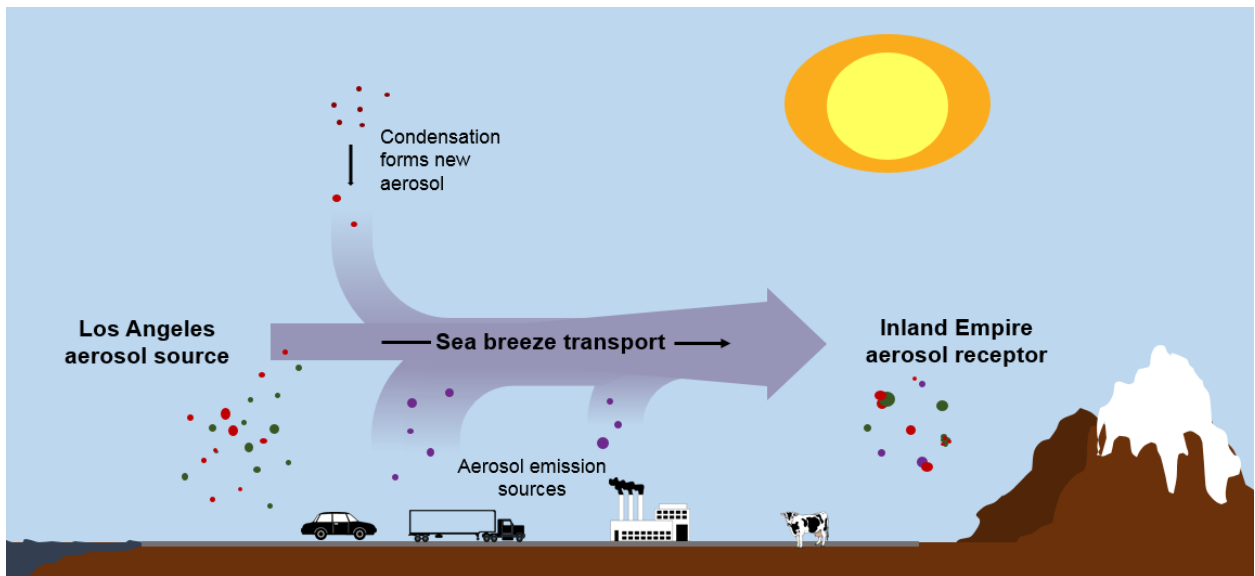
Figure I1. Westerly sea-breeze transports aerosol from Los Angeles to the Inland Empire. This aerosol evolves during transport, and takes on new particles. New aerosol can be emitted from primary sources such as cars or factories, or formed from condensing gases.

Characteristic westerly (eastern-moving) sea-breeze transports aerosol from coastal Los Angeles, an aerosol source region, into the Inland Empire, an aerosol receptor (Figure I1). This movement covers

approximately 50 miles, and takes between a day and a week[6,59]. With time and transport, this aerosol evolves by coagulation[60], chemical reactions[61–66], and water and VOC condensation[1,59]. Thus, aged aerosols trend towards larger average diameters and lower overall concentrations.[67] Aerosol at a downwind receptor will contain this aged, initial source population, as well as a mix local particles, and those incorporated during transport[1].

Three past campaigns[1,59,68] found significant increases in bulk aerosol between source and receptor regions[1,59], though the size-distribution of the receptor aerosol has varied between decades[1,59,68], In 1987, the Southern California Air Quality Study (SCAQS) showed a distinctly bimodal population in Riverside (a receptor region) with modes at approximately 250 and 650nm[68]. In a later study in 1996, Hughes et al. found only a single, larger mode at 500nm in Riverside[59]. In 2001, Fine et al. once again observed a bimodal population in the Inland Empire, but this time at smaller diameters: 45 and 140nm. All measurement were collected in the summer so it is unlikely that the changes are due to seasonal variations, though long-term climatic changes[69,70] could play a role.

Between major campaigns, this study provides an interim quantification of the size-distributions of aerosol in the Los Angeles source and Inland Empire receptor regions, as well as an analysis of their differences. We discuss these differences alongside a VOC analysis which compares the additional amount of bulk anthropogenic pollution and photo-oxidized anthropogenic VOCs present at receptor over source locations. Benzene and carbon dioxide are used to represent the total aerosol pollution at different locations, whether introduced in the source region, receptor region, or during transport. Both compounds are common anthropogenic emissions,[71] and due to their long atmospheric lifetimes[71,72] [73,74], would not react significantly during transport, and thus, increase with the introduction of new anthropogenic pollution. The level of photo-oxidized anthropogenic VOCs are represented by isopropyl nitrate. Isopropyl nitrate has no direct emission sources but is formed by the photo-oxidation of anthropogenic VOCs, and is thought to have a positive, linear relationship with anthropogenic SOA formation[75]. This VOC analysis is a simplified view of anthropogenic emissions and atmospheric processing. It is discussed here to provide context for the observed changes in aerosol between regions, rather than conclusions regarding their sources.

Results and Discussion

All days of this study had warm, clear, sunny weather. Characteristic westerly flow was confirmed using the NOAA HYSPLIT model as described in the methods section. No significant fires were reported in either source or receptor regions on the days of this study. Two minor fires were present in Central California in 2014, but were considered too small to contribute meaningfully to the studied aerosol. All measurements both years were made between a Tuesday morning and Thursday evening, avoiding the aerosol minimums often measured on Mondays resulting from the 24-hour delay in aerosol transport and reduced weekend traffic[1,59].

I.   Bulk aerosol of all measured sites

Source sites: Los Angeles, Los Alamitos, Long Beach
A typical aerosol population is log-normally size-distributed by both mass and concentration, and atmospheric aerosol exhibits log-normality over certain diameter ranges, such as the sub-micron range[60]. Source regions showed no distinct concentration modes in the measured 60-1000nm range either year (Figure R1). What may be the upper tail of a peak was observed in the small-end of the measured range in Los Angeles in 2013, and the largest measured concentration was at 60nm, the lower-bound of the measured range (Figure R1, panel A). This is consistent with findings that typical urban aerosol populations have concentration modes between 20-50nm[31–34], but different than the Long Beach aerosol measured by Hughes et al. in 1996[59] where particle concentrations reached maxima in the 200-600nm range, and decayed to almost nothing by 60nm.

In 2014, the four source measurements had similar aerosol concentrations and size distributions. Data from morning measurements were higher for both locations, consistent with previous studies of the area[1,68,76] and the increasing mixing layer depth through the day. All 2014 sources showed moderate concentration maxima near 60nm and 200nm, with total concentrations in the measured range between 13,840 particles cm^{-3} and 19,430 particles cm^{-3} (Table R1). This data suggests, like previous studies[31–34], that the majority of the Los Angeles aerosol may be in the especially toxic and less-regulated <200nm diameter range.

In 2014, all source measurements had calculated mass peaks at approximately 300nm (Figure R1, Panel D). Calculated particle mass for Los Angeles in 2013 had modes at approximately 200nm and 550nm (Figure R1, Panel B). Without knowing the composition of the measured aerosols, no statement can be made regarding their source. Overall, mass peaks in this study reached maxima between 15-25 ug m^3, lower than the 50-80 ug m^3 maxima measured in 1987 and 1996.

Receptor sites: March (in Riverside), Ontario, San Bernardino

All receptor sites in 2013 and 2014 showed similar concentration distributions, with a single mode between 70-90nm (Figure R1, Panels A and C), with one exception of a small second mode at 270nm in Ontario in 2014. Concentrations were approximately three-fold higher in 2013 than 2014 (Table R1). It is possible that a smaller, secondary mode is present below the measured range, though there is no clear evidence of convolvement with a second, smaller peak by speculation (Figure R1, Panels A and C). Bimodality has been observed in this region in the past, such as by Fine et al. in 2001, who measured two distinct modes at 45nm and 140nm, though the relative heights of these modes were heavily dependent on the time of day such that only minor bimodality was observed in the early mornings and late at night[1].

Overall, receptors in this study had more than double the mode concentrations observed by Fine et al[1] in 2001 at similar sampling sites, which never exceeded 140 particles cm^{-3} in Riverside and 310 particles cm^{-3} in Rubidoux. In 2013, the EPA 24-hour maximum of 35μg m^3 was exceeded in March in the morning, and save for the March measurement in 2014, all receptor sites exceeded the EPA 3-year maximum of 12 μg m^{-3} (Table R1).

In 2013, calculated mass in Ontario, March in the afternoon, and San Bernardino reach a maximum between 300-400nm, with more mass between 70-200nm than would be expected from a single log-normal distribution peaking at 300-400nm. The March morning mass distribution is bimodal, with one peak at approximately 85nm, and another at 280nm. Mass bimodality in this area was also observed by Hering et al in 1987 in August, but at larger diameters: 250nm and 650nm[68].

Though total concentration and mass vary between 2013 and 2014, the diameter of the modes remains relatively constant at receptor sites. This same consistency was observed in the summer of the three preceding studies, and overall, both concentration and mass modes appear at smaller diameters in this study than those preceding. The consistency in peak location in each study regardless of total concentration or mass, as well as the discrepancies between studies conducted approximately a decade apart, could suggest large-scale changes in aerosol processes in the Los Angeles Basin.

I.   Bulk aerosol of measured sites

A

B

C

D
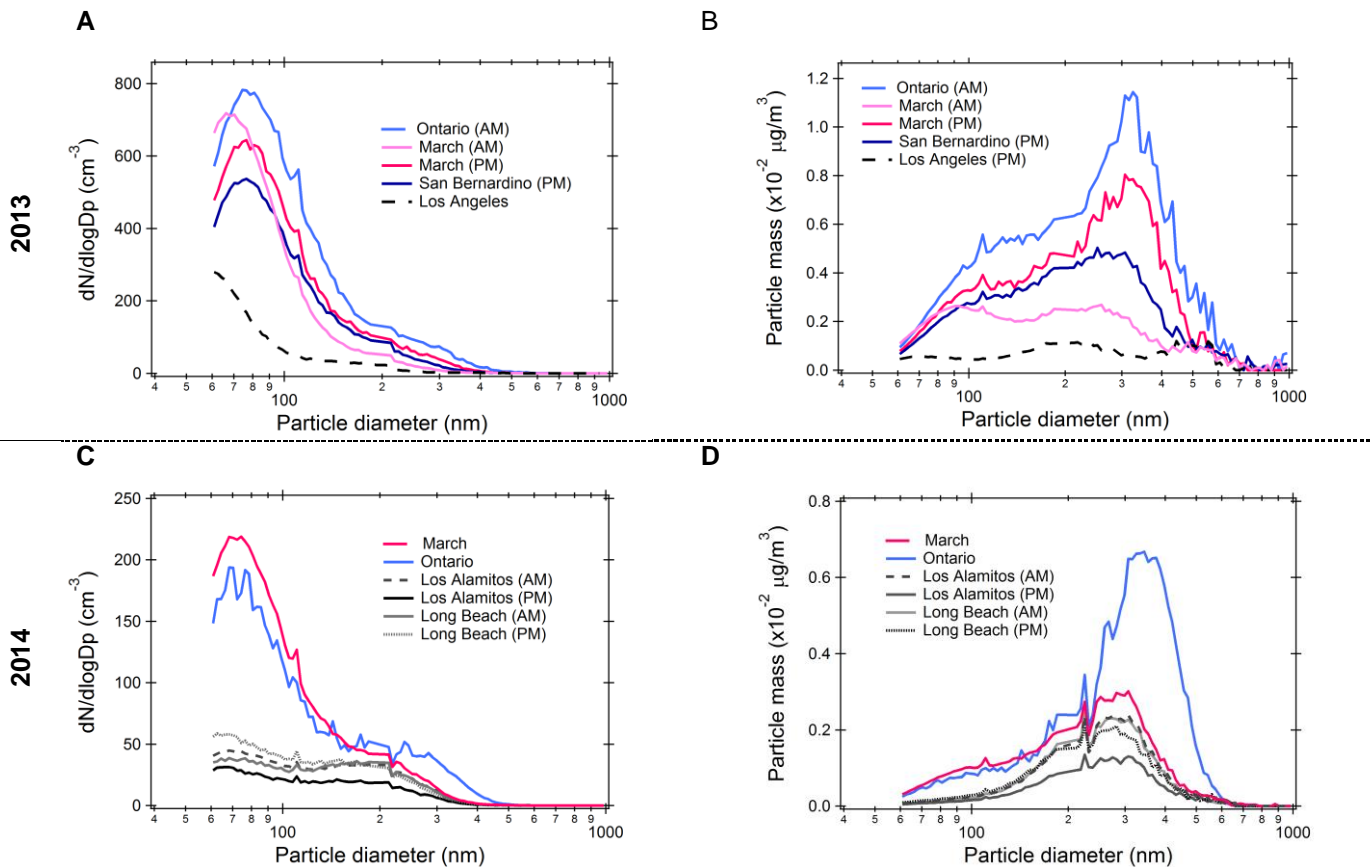
Figure R1. Individual log-normalized concentration (dN/dlogDp) (A, C) and mass (B, D) distributions of bulk aerosol populations for all missed approaches in 2013 (A, B) and 2014 (C, D).

		Totals over measured range		Peak of concentration distribution	
		conc. (cm^{-3})	mass (µg m^{-3})	diameter at peak	conc. at peak
2013	Los Angeles	4,010	5.77		
	San Bernardino	13,840	**22.33‡**	87	550
	March (PM)	14,450	**15.02**	74	470
	Ontario	16,400	**31.37**	86	790
	March (AM)	19,430	***38.65‡‡***	86	730
2014	Long Beach (AM)	1,230	6.63		
	Long Beach (PM)	1,870	3.90		
	Los Alamitos (PM)	2,150	6.51		
	Los Alamitos (PM)	1,840	6.15		
	March	5,630	10.26	70-75*	224**
	Ontario	5,750	***18.39‡***	70-75*	188**

Table R1. Total aerosol concentration and mass, and peak aerosol diameter for 2013 missed approaches. Source regions are shaded in grey, receptor regions are unshaded. Total values are sums over the measured 60-1000nm range. Peak diameters determined from lognormal fit equations calculated in Igor® Aerosol in source regions did not display a lognormal peak in the measured diameters ‡: Total masses in bold violate the EPA maximum not to be exceeded over a 3-year average. ‡‡: Total mass violates the EPA maximum not to be exceeded over a 24-hour average. *, **: due to subtly bi-modal distributions, no lognormal fit could be resolved for the March and Ontario 2014 data. The reported peak diameter range encompasses the maximum measured concentration (*) and concentration at peak reported is the maximum concentration measured in the raw data (**).

II. Changes evolved between source and receptor regions

Receptor locations had higher particle concentrations and mass in the measured range at all locations in both 2013 and 2014, with increases between 213 and 435 percent (Table R2). However, given the possibility of large concentrations in source locations below the measured range, this increase may not accurately represent changes to the entire aerosol populations. The largest contributions to added concentration in all locations occur at small diameters, between 70-110nm (Figure R2, panels A and C). A smaller, secondary concentration mode was observed at approximately 250nm in Ontario in 2014.

The new particle concentrations at small diameters found in this study may indicate different several things. It could come from the addition of fresh aerosol either in the source region or during transport, directly emitted for formed. This peak could also be the aged source aerosol population[67], smaller than the measured range of this study. Without knowing the composition of the added particles, this study cannot determine their source, though it is likely a mix of the above factors.

Total mass increases ranged from 77 to 637 percent (Table R2), which, given the minor mass contributions of small-diameter aerosols, is likely representative of mass increases over the total populations. The major mode for added mass in 2013 is in the 220-320nm range with a second, minor mode between 80-120nm. The only exception to this trend is the March afternoon measurement, where the smaller mode exceeds the larger (Figure R2, panel B). This could be due to an exchange between POA (larger mode) and SOA (smaller mode) moving from morning to afternoon, as was observed in Riverside by Fine et al. in 2001[1]. Kim et al. also attributed a large portion of the Riverside aerosol to local SOA[77]. However, this study makes no definitive statement regarding the source of this fluctuation. In 2014 only one measurement was taken at each receptor region, so no insight on these diurnal variations is available for that year.

I.   Changes evolved between source and receptor regions

A

B

C

D
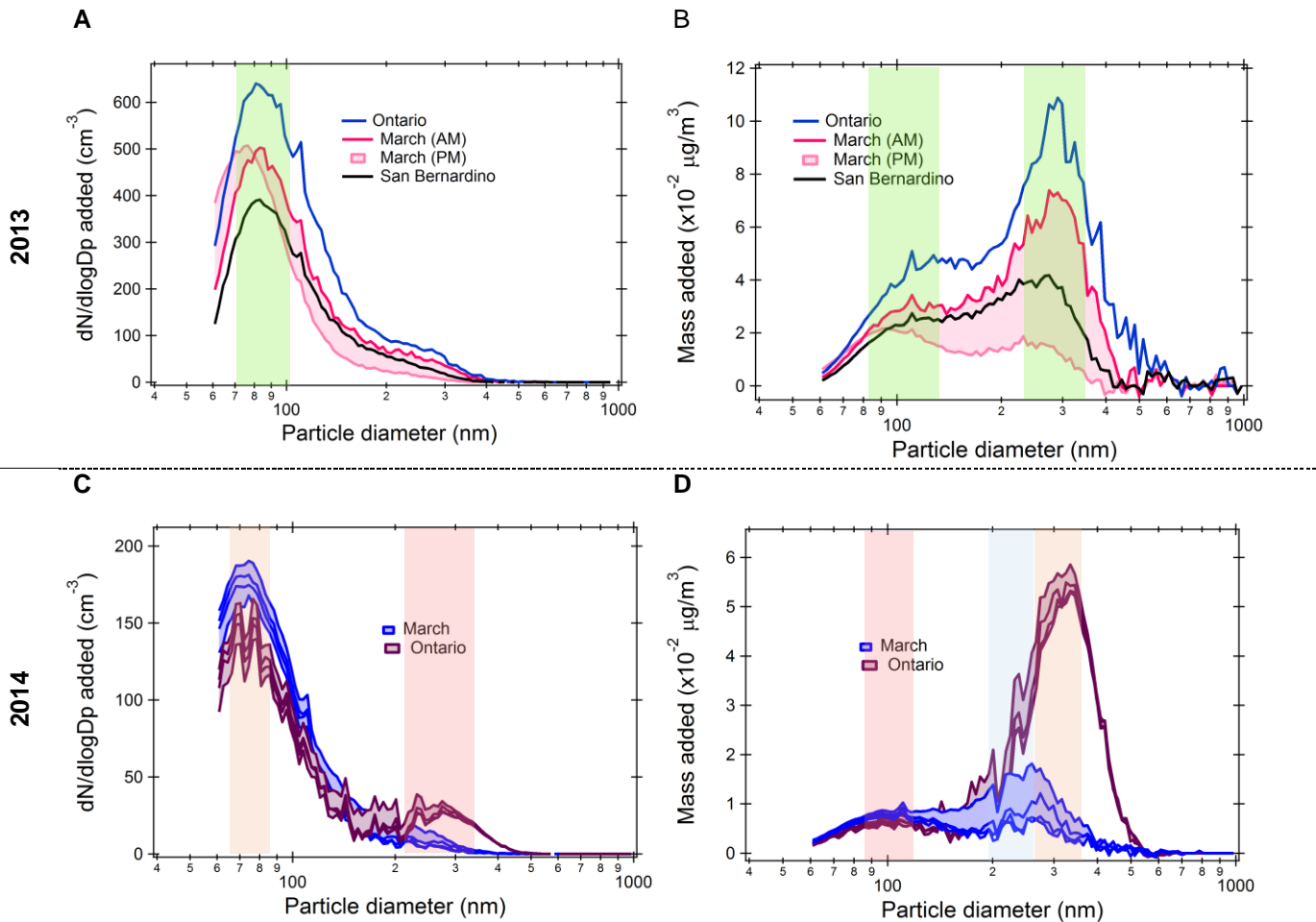
Figure R2. Differences in log-normalized concentration (dN/dlogDp, panels A, C) and mass (B, D) distributions of bulk aerosol populations between source and receptor sites for all missed approaches in 2013 (A, B) and 2014 (C, D). Diameter ranges of all peaks are shaded for accentuation. In cases when more than one trace corresponds to a single receptor region (March in 2013, both receptors in 2014), the area between them is shaded.

		Percent increase		Total increase	
	receptor	conc. (cm^{-3})	mass (µg m^{-3})	conc. (cm^{-3})	mass (µg m^{-3})
2013	San Bernardino	245	287	9,830	16.56
	March (PM)	261	160	10,450	9.25
	Ontario	435	637	17,430	36.71
	March (AM)	314	424	12,570	24.42
2014	March	232	77	12.570	4.46
	Ontario	213	217	17.430	12.59

Table R2. Differences in aerosol concentration and mass between individual source and receptor regions. In 2014, when four source-region missed approaches were performed, reported values are averages over all individual differences. In 2013 only one source-region missed approach was performed (LAX) so reported values are exact differences.

III. VOC analysis for context

This study found a general positive correlation between the additional mass and additional bulk pollution tracer levels measured at the receptor locations. A possible positive correlation was observed between additional isopropyl nitrate and particle mass at the receptors. These results indicate, as is expected, that the addition of particle mass between source and receptor regions is positively correlated with increases in anthropogenic pollution, as well as the ambient levels of photo-oxidized anthropogenic pollution. This VOC data cannot determine whether the pollution or particle mass was added in transport or at the receptor location.
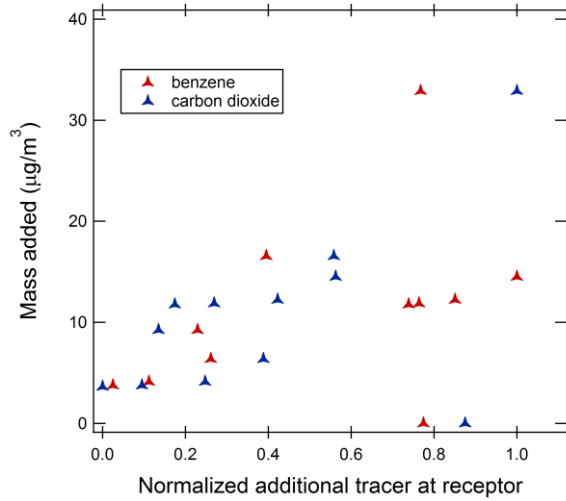
Figure R3a. The general positive correlation between amount of anthropogenic pollution tracers carbon dioxide and benzene present in excess at each receptor site over each source site, and amount of aerosol mass added between the same two regions. Differences are normalized by division over the largest total difference.
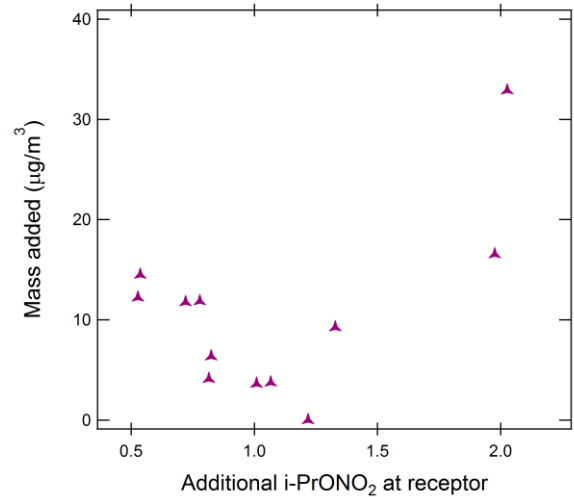
Figure R3b. A possible positive correlation between the amount of isopropyl nitrate found in receptor sites over source sites and the amount of mass added between those same two locations.

Conclusions

The NASA SARP 2013 and 2014 campaigns found universal increases in particle mass and concentration between the Los Angeles source region and the Inland Empire receptor region in the 60-1000nm diameter range. 70-110nm diameter aerosol accounts for the majority of the observed additions at receptor sites. The differences in receptor and source aerosol are likely a combination of locally emitted and transported anthropogenic SOA and POA. In the source sites, no concentration peak could be resolved, which suggests the presence of concentration modes below the 60nm minimum measured in this campaign. Unlike previous studies, receptor region aerosols in this study are unimodal, though a second mode may be present below the measured range. If this bimodality in fact is the case, this study as well as three similar ones preceding, show a decreasing diameter trend in Inland Empire aerosol. Given the enhanced toxicity of ultrafine aerosol, this is concerning and merits further study.

Methods

General considerations

Particle and VOC were collected onboard the NASA DC-8 Airborne Laboratory during the NASA Student Airborne Research Program flight campaigns in June of 2013 and 2014. Flights were based out of the NASA Armstrong Flight Research Center in Palmdale, California. Source and receptor regions were characterized by averages over mixed-layer vertical profiles from individual missed approaches (Figure M1) at six sampling sites, three in each region (Figure M2). Dates, times, and locations of each measurement can be found in Table M1. Particle data were measured from a continuous flow of inlet air. (See *Instrumentation,* pg. 17).

Characteristic westerly flow was confirmed for all locations and specific times of this study using meteorological trajectories from the National Oceanic Atmospheric Administration Hybrid Single Particle Lagrangian Integrated Trajectory (NOAA HYSPLIT) meteorological model using data sets from the North American Mesoscale 12km resolution meteorological model (NAM12). Forward trajectories were run at the time of each missed approach for each of three starting locations independently, covering an approximately half-mile square over each source location to confirm the westerly movement of the measured aerosol into the Inland Empire receptor region. Backward trajectories were run for the receptor region missed approaches to confirm the coastal Los Angeles origin of the measured aerosol by the same method. Aerosol measurements consider a low-elevation window of air, from a series of rapid (1-2 minutes) descents from high elevations (>5,000 feet) to ground level (<200 feet) and back up to high elevation; maneuvers known as "missed approaches." The coastal Los Angeles pollution source region was characterized by missed approaches at the Los Angeles International Airport (LAX), Los Alamitos Army Airfield and Long Beach International Airport; and the Inland Empire pollution receptor region, by the Ontario International Airport, San Bernardino International Airport, and March Air Army Reserve in Riverside.

Table M1. Times and locations of missed approaches

Time of missed approach (PDT)			*Sampling site*	
			Location	*Source/Receptor*
2013	June 18	9:45	Ontario	Receptor
		9:54	March	Receptor
		10:11	San Bernardino	Receptor
	June 19	17:19	LAX	Source
	June 19	17:44	March	Receptor
2014	June 23	9:32	Los Alamitos	Source
		9:50	Long Beach	Source
		15:01	Los Alamitos	Source
		15:10	Long Beach	Source
		10:12	Ontario	Receptor
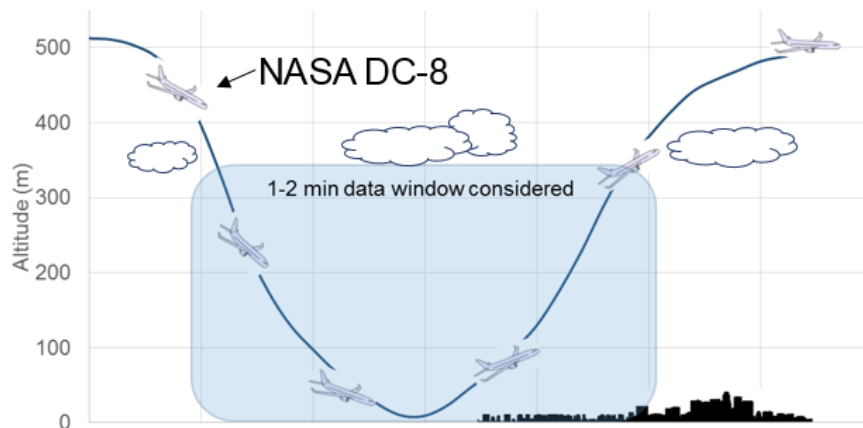
Figure M1. A typical missed-approach flight path, shown above, surveys low elevation air.

Figure M2. The studied area. Source and receptor regions (blue shaded), sampling sites (red stars) and 12-hour NOAA HYSPLIT trajectories for the days of the flights (red lines), are indicated.

Restricting the data window to time in the mixed layer

Potential temperature is constant in the mixed layer. Potential temperature was plotted against radar altitude for all missed approaches. Boundaries of the plateau were graphically determined, and converted to a time-window. Only data from this time-window were considered (Figure M4).

Potential temperature was calculated by:

$$\theta = T \left(\frac{Po}{P}\right)^{\frac{R}{Cp}}$$

P_o = standard reference pressure, 1000 milibars
P = ambient fluid pressure
R = the gas constant, 8.31445 J K^{-1} mol^{-1}
C_p = 29.07 K mol J^{-1}, the specific heat capacity of air at a constant pressure

Equation 1. Potential temperature

Mixed layer depths were compared with the projected depths for the time and location of the missed approaches from NOAA HYSPLIT meteorological trajectories using data sets from the NAM12km model.

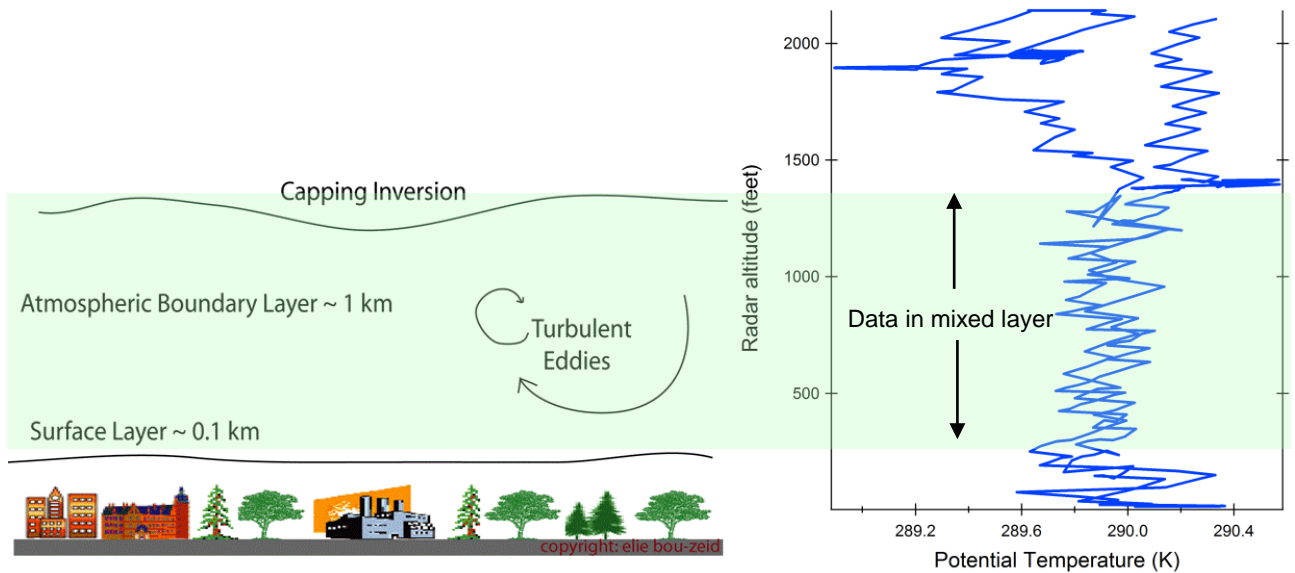**Figure M3.** The mixed layer, a low-elevation layer of air that is constantly being stirred by turbulent eddies, compared to a plot of potential temperature versus radar altitude, illustrating the characteristic plateau in potential temperature in the mixed layer. Only data in shaded region was considered.

Particle data

Instrumentation: the DMT-UHSAS

Particle measurements were made using a Droplet Measurement Technologies Ultra High Sensitivity Aerosol Spectrometer (DMT-UHSAS), which measures the number of particles within pre-specified diameter-ranges. It consists of five subunits (Figure M4a).:

(1) *Optical system* (Figure M4b,c): particles are illuminated by and scatter a Nd^{3+}:YLG solid-state laser build around an Nd^{3+}:YLG active laser crystal on a 1054nm laser line. Scattering is detected by two pairs of Mangin collection optics. The primary scattering detection system images onto an avalanche photodiode (APD) to measure the smallest particles. Larger particles are measured by the secondary scattering system, which images to a low-gain PIN photodiode. Each detector is amplified in a current-to-voltage stage and fed into the analog electronics system.

(2) *Flow system*: a pumps pulls on an exhaust jet, pulling inlet jet across the laser at a user-fixed flow-rate. The inlet jet is focused and directed through the optical-unit laser.

(3) *Analog electronics system:* amplifies and processes the particle signal from both ADP and PIN photodiodes. Particle signal is fed into two detectors, each with two different gains (Table M2). The gain ratios amplify the pure electrical signal, and low-pass filter the data.

Table M2. Gains of the two DMT-UHSAS detectors		
	High gain	Low gain
Primary detector	G3	G2
Secondary detector	G1	G0

With gain ratios:

$$\frac{G3}{G2} = 50 \ , \frac{G2}{G1} = \frac{G1}{G0} = 20$$

(4) *Digital electronics system:* converts each of the four gain stages from analog to digital, and analyzes particle signals and maps to one of up to 99 pre-specified size-bins between 50nm and 1000nm diameter

(5) *On-board PC monitor:* provides a user-interface.

This study measured particles in the 60-1000nm diameter range in 99 logarithmically-spaced size bins. Data were collected at a frequency of 10Hz.
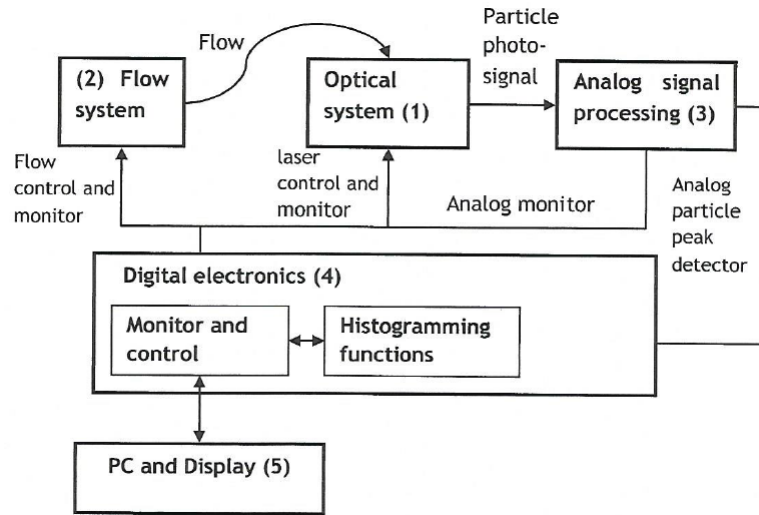
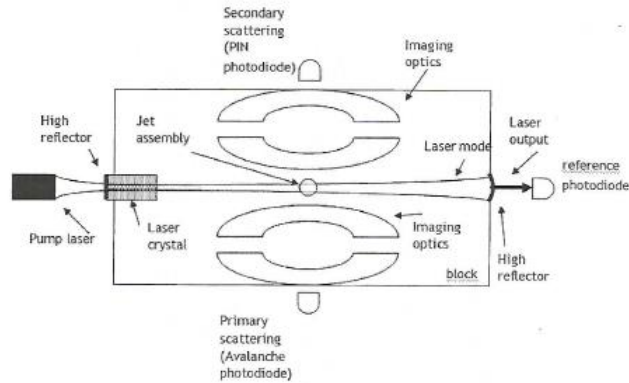**Figure M4a.** Box-schematic of the DMT-UHSAS, with the five subunits labeled.

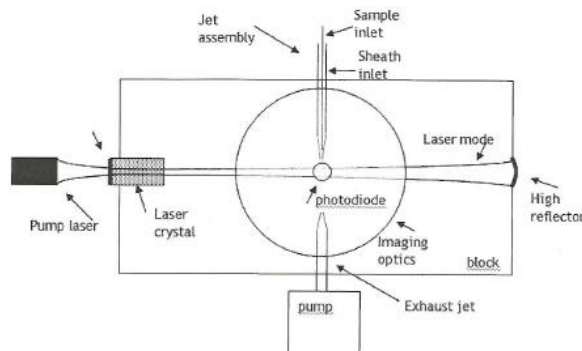**Figure M4b.** Top-view of optical block subunit

Figure M4c. Side-view of optical block subunit

Particle data processing

Particle data were processed using MatLab 7 and IgorPro®, in four general stages, outlined below.

(i) Removing rare erroneous measurements: Within the particle data, there were two minor sources of erroneous values: missed measurements of a single size-bin in a single scan, recorded as "error," and falsely inflated individual measurements of small-diameter (60-150mn) particles due to minor instrument drift between calibrations. Both sources of erroneous values are expected from the DMT-UHSAS and highly infrequent, accounting for less than 0.1% of the total data set. Individual missed measurements were replaced with the average value of the measurements in each of the adjacent size bins. i.e. if no measurement was recorded for the 65nm size bin, the value of this bin was assigned the average of the values in the 64 and 66nm size bins. Typical particle maxima did not exceed 10,000 counts after log-normalization. Thus, any measurement over 10,000 particles was considered false inflated and reassigned a value of zero.

(ii) Converting particle counts to concentration and mass: Particle counts were converted to concentration by the following formula:

$$\frac{particles}{sccm} = \frac{particle\ counts}{50\left(\frac{sccm}{min}\right)} * \frac{1min}{60sec} * \frac{10samples}{sec}$$

Equation 2. Conversion from particle flow to concentration

Particle mass was calculated from particle concentration assuming spherical particles with a density of 1 g sccm^{-1}. This density is precedented in literature for sub-micron particles the region of this study, as is a relatively consistent density of aerosol in this location and diameter range.[68]

(iii) Averaging the mixed-layer data window: All of the data presented in this study are averages over a single missed approach, spanning one to two minutes of data, and 600-1200 individual DMT-UHSAS scans. Because of the homogenous nature of the mixed layer, it was expected that averages over these windows would be representative of the particle population throughout a missed approach. To validate this, particle peak diameter and total particle count overall size bins were plotted against time through each missed approach. As anticipated, both total particle population and peak diameter were consistent throughout the mixed layer for the missed approaches.

(iv) Fitting averaged traces to logarithmic curves to determine peak counts: The concentrations of typical, poly-disperse aerosol populations are normally distributed over a logarithmic diameter scale. Concentrations discussed in this study are log-normalized, as is typical for aerosol studies. Log-normal concentrations are labeled as dN/dlogDp. Normalized concentration was calculated by the standard formula:

$$\frac{dN}{dlogDp} = \frac{dN}{logDp,u - logDp,l}$$

dN = measured particle concentration
Dp,u = upper bound diameter
Dp,l = lower bound diameter

Equation 3. Log-normalized particle concentration

Next, log-normal curves were fit to the data using a normal curve equation modified for a logarithmic x-scale, to account for the log-normal nature of aerosol distributions. Lognormal curve fitting was done using both MATLAB 7 polyfit and Igor® QuickFit function to confirm fit accuracy. All fits used the standard lognormal equation:

$$\frac{dN}{dlogDp} = y_o + A[-\left(\frac{\log\left(\frac{x}{x_o}\right)}{width}\right)^2]$$

x = particle diameter
x_o = mean particle diameter = peak particle diameter
width = the full width of the normal curve at half of its maximum value
A = amplitude scaling factor
y_o = added constant dN/dlogDp, theoretically = 0

Equation 4. Log-normal fit-curves

Source regions did not peak in the measured range, and were not fit to log-normal curves. No maximum was determined for these measurements.

Comparing individual differences between sources and receptors

Changes in the aerosol between source and receptor regions are the mathematical differences between individual source and receptor regions measured in a particular year.

VOC Measurements: Whole Air Samples

VOC levels were measured from Whole Air Samples taken simultaneously with particle data during missed approaches. For each sample, stainless steel cans were evacuated and then filled to a pressure of 30psi from a flow of ambient air inlet from immediately outside of the DC-8. During missed approaches, cans were filled at approximately 60 second intervals, each representing approximately 30 seconds or air time, or a 1-3km flight-path. Within two weeks of collection, VOC levels were measured in the lab via gas chromatography (GC). The GC system used comprised of three high-pressure 5890 GCs. Samples were split to 6 different columns and then sent to one of three possible detectors: flame ionization for benzene, mass spectrometry for isopropyl nitrate, and thermal conductivity for carbon dioxide. Values reported in this study are averages over all cans taken within the mixed layer during a single missed approach. All VOC data in this study is courtesy of the Rowland-Blake Laboratories at the University of California Irvine.

Differences between source and receptor regions were calculated by subtracting the total particle mass (hypothesized dependent variable), or the measured VOC level (independent variable), from a single source measurement from a single receptor measurement for all source-receptor combinations within a given year. Benzene and carbon dioxide differences were then normalized by division over the largest measured difference.

Acknowledgements

References

1. Fine, P. M., Shen, S. & Sioutas, C. Inferring the Sources of Fine and Ultrafine Particulate Matter at Downwind Receptor Sites in the Los Angeles Basin Using Multiple Continuous Measurements Special Issue of *Aerosol Science and Technology* on Findings from the Fine Particulate Matter Supersites Program. *Aerosol Sci. Technol.* **38,** 182–195 (2004).

2. O'Dowd, C. D. & de Leeuw, G. Marine aerosol production: a review of the current knowledge. *Philos. Trans. R. Soc. Math. Phys. Eng. Sci.* **365,** 1753–1774 (2007).

3. Costabile, F. *et al.* Spatio-temporal variability and principal components of the particle number size distribution in an urban atmosphere. *Atmospheric Chem. Phys.* **9,** 3163–3195 (2009).

4. Mohr, C. *et al.* Characterization of Primary Organic Aerosol Emissions from Meat Cooking, Trash Burning, and Motor Vehicles with High-Resolution Aerosol Mass Spectrometry and Comparison with Ambient and Chamber Observations. *Environ. Sci. Technol.* **43,** 2443–2449 (2009).

5. Riipinen, I. *et al.* Organic condensation: a vital link connecting aerosol formation to cloud condensation nuclei (CCN) concentrations. *Atmospheric Chem. Phys.* **11,** 3865–3878 (2011).

6. Pandis, S. N., Harley, R. A., Cass, G. R. & Seinfeld, J. H. Secondary organic aerosol formation and transport. *Atmospheric Environ. Part Gen. Top.* **26,** 2269–2282 (1992).

7. Haywood, J. & Boucher, O. Estimates of the direct and indirect radiative forcing due to tropospheric aerosols: A review. *Rev. Geophys.* **38,** 513 (2000).

8. Kaufman, Y. J. Smoke and Pollution Aerosol Effect on Cloud Cover. *Science* **313,** 655–658 (2006).

9. Charlock, T. P. & Sellers, W. D. Aerosol, Cloud Reflectivity and Climate. *J. Atmospheric Sci.* **37,** 1136–1137 (1980).

10. Andreae, M. O. & Rosenfeld, D. Aerosol–cloud–precipitation interactions. Part 1. The nature and sources of cloud-active aerosols. *Earth-Sci. Rev.* **89,** 13–41 (2008).

11. Larson, S. M., Cass, G. R. & Gray, H. A. Atmospheric Carbon Particles and the Los Angeles Visibility Problem. *Aerosol Sci. Technol.* **10,** 118–130 (1989).

12. Wolff, G. T., Ferman, M. A., Kelly, N. A., Stroup, D. P. & Ruthkosky, M. S. The Relationships Between the Chemical Composition of Fine Particles and Visibility in the Detroit Metropolitan Area. *J. Air Pollut. Control Assoc.* **32,** 1216–1220 (1982).

13. Appel, B. R., Tokiwa, Y., Hsu, J., Kothny, E. L. & Hahn, E. Visibility as related to atmospheric aerosol constituents. *Atmospheric Environ. 1967* **19,** 1525–1534 (1985).

14. Zhang, X. ., McMurray, P. ., Hering, S. . & Casuccio, G. . Mixing characteristics and water content of submicron aerosols measured in Los Angeles and at the grand canyon. *Atmospheric Environ. Part Gen. Top.* **27,** 1593–1607 (1993).

15. Eldering, A., Cass, G. R. & Moon, K. C. An air monitoring network using continuous particle size distribution monitors: Connecting pollutant properties to visibility via Mie scattering calculations. *Atmos. Environ.* **28,** 2733–2749 (1994).

16. Horvath, H. Estimation of the average visibility in central Europe. *Atmos. Environ.* **29,** 241–246 (1995).

17. Oberdörster, G., Oberdörster, E. & Oberdörster, J. Nanotoxicology: an emerging discipline evolving from studies of ultrafine particles. *Environ. Health Perspect.* **113,** 823–839 (2005).

18. Künzli, N. *et al.* Breathless in Los Angeles: The Exhausting Search for Clean Air. *Am. J. Public Health* **93,** 1494–1499 (2003).

19. Pope III, C. A. Lung Cancer, Cardiopulmonary Mortality, and Long-term Exposure to Fine Particulate Air Pollution. *JAMA* **287,** 1132 (2002).

20. Martuzzi, M., World Health Organization. & Regional Office for Europe. *Health impact of PM$_{10}$ and ozone in 13 italian cities.* (World Health Organization Europe, 2006).

21. Peters, J. M. *et al.* A study of twelve Southern California communities with differing levels and types of air pollution. I. Prevalence of respiratory morbidity. *Am. J. Respir. Crit. Care Med.* **159,** 760–767 (1999).

22. Ito, K., Thurston, G. D., Hayes, C. & Lippmann, M. Associations of London, England, Daily Mortality with Particulate Matter, Sulfur Dioxide, and Acidic Aerosol Pollution. *Arch. Environ. Health Int. J.* **48,** 213–220 (1993).

23. Seaton, A., MacNee, W., Donaldson, K. & Godden, D. Particulate air pollution and acute health effects. *Lancet* **345,** 176–178 (1995).

24. Etzel, R. A. Air Pollution and Bronchitic Symptoms in Southern California Children with Asthma. *Environ. Health Perspect.* **107,** 691 (1999).

25. Gauderman, W. J. *et al.* Association between air pollution and lung function growth in southern California children. *Am. J. Respir. Crit. Care Med.* **162,** 1383–1390 (2000).

26. Gauderman, W. J. *et al.* Association between air pollution and lung function growth in southern California children: results from a second cohort. *Am. J. Respir. Crit. Care Med.* **166,** 76–84 (2002).

27. Xia, T. *et al.* Quinones and aromatic chemical compounds in particulate matter induce mitochondrial dysfunction: implications for ultrafine particle toxicity. *Environ. Health Perspect.* **112,** 1347–1358 (2004).

28. Faiola, C. *et al.* Ultrafine Particulate Ferrous Iron and Anthracene Associations with Mitochondrial Dysfunction. *Aerosol Sci. Technol.* **45,** 1109–1122 (2011).

29. Lighty, J. S., Veranth, J. M. & Sarofim, A. F. Combustion Aerosols: Factors Governing Their Size and Composition and Implications to Human Health. *J. Air Waste Manag. Assoc.* **50,** 1565–1618 (2000).

30. Li, N. *et al.* Use of a stratified oxidative stress model to study the biological effects of ambient concentrated and diesel exhaust particulate matter. *Inhal. Toxicol.* **14,** 459–486 (2002).

31. Harrison, R. M. *et al.* Measurement of number, mass and size distribution of particles in the atmosphere. *Philos. Trans. R. Soc. Math. Phys. Eng. Sci.* **358,** 2567–2580 (2000).

32. Morawska, L., Thomas, S., Bofinger, N., Wainwright, D. & Neale, D. Comprehensive characterization of aerosols in a subtropical urban atmosphere. *Atmos. Environ.* **32,** 2467–2478 (1998).

33. Hughes, L. S., Cass, G. R., Gone, J., Ames, M. & Olmez, I. Physical and Chemical Characterization of Atmospheric Ultrafine Particles in the Los Angeles Area. *Environ. Sci. Technol.* **32,** 1153–1161 (1998).

34. Woo, K. S., Chen, D. R., Pui, D. Y. H. & McMurry, P. H. Measurement of Atlanta Aerosol Size Distributions: Observations of Ultrafine Particle Events. *Aerosol Sci. Technol.* **34,** 75–87 (2001).

35. Chow, J. C. *et al.* PM $_{2.5}$ chemical composition and spatiotemporal variability during the California Regional PM $_{10}$ /PM $_{2.5}$ Air Quality Study (CRPAQS). *J. Geophys. Res.* **111,** (2006).

36. Newman, P. *Sustainability and cities: overcoming automobile dependence*. (Island Press, 1999).

37. Schiferl, L. D. *et al.* An investigation of ammonia and inorganic particulate matter in California during the CalNex campaign: CALNEX AMMONIA AND INORGANIC FINE PM. *J. Geophys. Res. Atmospheres* **119,** 1883–1902 (2014).

38. *Public Hearing to Consider Amendments to the Ambient Air Quality Standards for Particulate Matter and Sulfates: Staff Report.* Sacramento, Calif: Air Resources Board, California Environmental Protection Agency; 2002.

39. *Final Report to Congress on Benefits and Costs of the Clean Air Act, 1970- 1990*. Washington, DC: US Environmental Protection Agency; 1997. EPA publication 410-R-97-002.

40. *Regulatory Impact Analysis-Heavy- Duty Engine and Vehicle Standards and Highway Diesel Fuel Sulfur Control Requirements.* Washington, DC: US Environmental Protection Agency; 2000. EPA publication 420-R-00-026.

41. Aan de Brugh, J. M. J. *et al.* Modelling the partitioning of ammonium nitrate in the convective boundary layer. *Atmospheric Chem. Phys.* **12,** 3005–3023 (2012).

42. Nilsson, E. D., Rannik, U., Kulmala, M., Buzorius, G. & O'Dowd, C. D. Effects of continental boundary layer evolution, convection, turbulence and entrainment, on aerosol formation. *Tellus B* **53,** 441–461 (2001).

43. Gustafson Jr, W. I., Berg, L. K., Easter, R. C. & Ghan, S. J. The Explicit-Cloud Parameterized-Pollutant hybrid approach for aerosol–cloud interactions in multiscale modeling framework models: tracer transport results. *Environ. Res. Lett.* **3,** 025005 (2008).

44. Feng, Y. Effects of cloud overlap in photochemical models. *J. Geophys. Res.* **109,** (2004).

45. Tang, Y. Impacts of aerosols and clouds on photolysis frequencies and photochemistry during TRACE-P: 2. Three-dimensional study using a regional chemical transport model. *J. Geophys. Res.* **108,** (2003).

46. Ervens, B., Turpin, B. J. & Weber, R. J. Secondary organic aerosol formation in cloud droplets and aqueous particles (aqSOA): a review of laboratory, field and model studies. *Atmospheric Chem. Phys.* **11,** 11069–11102 (2011).

47. Fahey, K. M. & Pandis, S. N. Optimizing model performance: variable size resolution in cloud chemistry modeling. *Atmos. Environ.* **35,** 4471–4478 (2001).

48. Wang, H. *et al.* Sensitivity of remote aerosol distributions to representation of cloud–aerosol interactions in a global climate model. *Geosci. Model Dev.* **6,** 765–782 (2013).

49. Yang, Q. *et al.* Impact of natural and anthropogenic aerosols on stratocumulus and precipitation in the Southeast Pacific: a regional modelling study using WRF-Chem. *Atmospheric Chem. Phys.* **12,** 8777–8796 (2012).

50. Barth, M. C. *et al.* Cloud-scale model intercomparison of chemical constituent transport in deep convection. *Atmospheric Chem. Phys.* **7,** 4709–4731 (2007).

51. Fast, J. D. *et al.* Modeling regional aerosol and aerosol precursor variability over California and its sensitivity to emissions and long-range transport during the 2010 CalNex and CARES campaigns. *Atmospheric Chem. Phys.* **14,** 10013–10060 (2014).

52. Held, T., Ying, Q., Kleeman, M. J., Schauer, J. J. & Fraser, M. P. A comparison of the UCD/CIT air quality model and the CMB source–receptor model for primary airborne particulate matter. *Atmos. Environ.* **39,** 2281–2297 (2005).

53. Spracklen, D. V. *et al.* Aerosol mass spectrometer constraint on the global secondary organic aerosol budget. *Atmospheric Chem. Phys.* **11,** 12109–12136 (2011).

54. Hodzic, A. *et al.* Limited influence of dry deposition of semivolatile organic vapors on secondary organic aerosol formation in the urban plume: IMPACT OF DRY DEPOSITION OF VOCs ON SOA. *Geophys. Res. Lett.* **40,** 3302–3307 (2013).

55. Volkamer, R. *et al.* Secondary organic aerosol formation from anthropogenic air pollution: Rapid and higher than expected. *Geophys. Res. Lett.* **33,** (2006).

56. Tuch, T. M. *et al.* Weak correlation of ultrafine aerosol particle concentrations <800 nm between two sites within one city. *J. Expo. Sci. Environ. Epidemiol.* **16,** 486–490 (2006).

57. Ketzel, M. *et al.* Particle size distribution and particle mass measurements at urban,near-city and rural level in the Copenhagen area and Southern Sweden. *Atmospheric Chem. Phys.* **4,** 281–292 (2004).

58. Bukowiecki, N., Dommen, J., Prévôt, A. S. H., Weingartner, E. & Baltensperger, U. Fine and ultrafine particles in the Zürich (Switzerland) area measured with a mobile laboratory: an assessment of the seasonal and regional variation throughout a year. *Atmospheric Chem. Phys.* **3,** 1477–1494 (2003).

59. Hughes, L. S. *et al.* Size and Composition Distribution of Atmospheric Particles in Southern California. *Environ. Sci. Technol.* **33,** 3506–3515 (1999).

60. Willeke, K. & Whitby, K. T. Atmospheric Aerosols: Size Distribution Interpretation. *J. Air Pollut. Control Assoc.* **25,** 529–534 (1975).

61. Calvert, J. G., Su, F., Bottenheim, J. W. & Strausz, O. P. Mechanism of the homogeneous oxidation of sulfur dioxide in the troposphere. *Atmospheric Environ. 1967* **12,** 197–226 (1978).

62. Stelson, A. W., Friedlander, S. K. & Seinfeld, J. H. A note on the equilibrium relationship between ammonia and nitric acid and particulate ammonium nitrate. *Atmospheric Environ. 1967* **13,** 369–371 (1979).

63. Stelson, A. W. & Seinfeld, J. H. Thermodynamic prediction of the water activity, NH4NO3 dissociation constant, density and refractive index for the NH4NO3-(NH4)2SO4-H2O system at 25°C. *Atmospheric Environ. 1967* **16,** 2507–2514 (1982).

64. Russell, A. G., McRae, G. J. & Cass, G. R. Mathematical modeling of the formation and transport of ammonium nitrate aerosol. *Atmospheric Environ. 1967* **17,** 949–964 (1983).

65. Russell, A. G. & Cass, G. R. Verification of a mathematical model for aerosol nitrate and nitric acid formation and its use for control measure evaluation. *Atmospheric Environ. 1967* **20,** 2011–2025 (1986).

66. Ebert, M., Weinbruch, S., Hoffmann, P. & Ortner, H. M. The chemical composition and complex refractive index of rural and urban influenced aerosols determined by individual particle analysis. *Atmos. Environ.* **38,** 6531–6545 (2004).

67. Max Zhang, K. & Wexler, A. S. Modeling the number distributions of urban and regional aerosols: theoretical foundations. *Atmos. Environ.* **36,** 1863–1874 (2002).

68. Hering, S., Eldering, A. & Seinfeld, J. H. Bimodal character of accumulation mode aerosol mass distributions in Southern California. *Atmos. Environ.* **31,** 1–11 (1997).

69. Cook, E. R. Long-Term Aridity Changes in the Western United States. *Science* **306,** 1015–1018 (2004).

70. Intergovernmental Panel on Climate Change. *Climate change 2001: the scientific basis: contribution of Working Group I to the third assessment report of the Intergovernmental Panel on Climate Change*. (Cambridge University Press, 2001).

71. Fortin, T. J. *et al.* Temporal Changes in U.S. Benzene Emissions Inferred from Atmospheric Measurements. *Environ. Sci. Technol.* **39,** 1403–1408 (2005).

72. *Draft technical support document: control of emissions of hazardous air pollutants from...* (Not Avail, 2013).

73. Archer, D. & Brovkin, V. The millennial atmospheric lifetime of anthropogenic CO2. *Clim. Change* **90,** 283–297 (2008).

74. Eby, M. *et al.* Lifetime of Anthropogenic Climate Change: Millennial Time Scales of Potential CO$_2$ and Surface Temperature Perturbations. *J. Clim.* **22,** 2501–2511 (2009).

75. De Gouw, J. A. *et al.* Sources of particulate matter in the northeastern United States in summer: 1. Direct emissions and secondary formation of organic matter in urban plumes. *J. Geophys. Res.* **113,** (2008).

76. Hughes, L. S. *et al.* Evolution of Nitrogen Species Air Pollutants along Trajectories Crossing the Los Angeles Area. *Environ. Sci. Technol.* **36,** 3928–3935 (2002).

77. Kim, S., Shen, S. & Sioutas, C. Size distribution and diurnal and seasonal trends of ultrafine particles in source and receptor sites of the Los Angeles basin. *J. Air Waste Manag. Assoc. 1995* **52,** 297–307 (2002).